New directions in thermoelectric and thermal-electric cooling

Andrey Gunawan, Aravindh Rajan, David M. Rodin, Patrick Creamer, Shannon K. Yee*
George W. Woodruff School of Mechanical Engineering, Georgia Institute of Technology, Atlanta, GA USA 30332

ABSTRACT

Conventional thermoelectric coolers have been widely used for cooling of electronic devices. Utilizing bismuth telluride materials, these Peltier modules are typically categorized as high heat flux devices that can achieve modest temperature differences in a compact architecture. Breaking from convention of typical bismuth telluride thermoelectric devices, an alternative method of providing thermal-electric cooling will be discussed providing inspiration for new cooling directions and materials challenges. While this approach has application in electric cooling of solids, there are also wider applications including space cooling and heat pumping.

Keywords: thermo-electrochemical, thermogalvanic, cooling

1. INTRODUCTION

Thermoelectric cooling remains an inviting subject for research, given the renewed emphasis on energy efficiency and carbon emissions reduction. The U.S. Department of Energy (DOE) has recently identified thermoelectric and other non-vapor compression heating, ventilation and air conditioning (HVAC) technologies to be the future of low-global warming potential (low-GWP) cooling technologies, because of their potential energy savings.[1] Thermoelectric coolers (TECs) use the Peltier effect to convert electrical input power into a heat flux. TECs have the potential to be used a low-GWP cooling technology due to the reliability, scalability, and solid-state nature of thermoelectrics,[2-4] but high costs and relatively low performance has restricted the commercial use of TECs to niche applications.[3, 5] An alternative to thermoelectric devices are thermo-electrochemical coolers.

Electrochemistry-based coolers have recently received significant attention because of its immense potential in reducing environmental impact and operating with high efficiency.[1] One example of this technology, which achieves up to one order of magnitude improvement over thermoelectric systems, has been published recently.[6] Motivated by this result, we are exploring another concept inspired by a Vanadium flow battery that uses electrochemical heat absorption to produce cooling. A simple thermal-electrochemical finite difference model is developed to find optimum operating parameters, namely flowrate of the electrolyte and current density. We are currently in the process of designing and fabricating the test cell.

2. THERMO-ELECTROCHEMICAL COOLING

Electrochemical cooling uses the heat absorption process that is present in redox reactions. The cooling load of such a process is dependent on the kinetics and the temperature coefficients of the redox couples involved. The latter is very similar to the Seebeck coefficient in thermoelectric materials. Here, we envision a vanadium flow battery inspired device that uses electrochemical heat absorption to cool an incoming water stream.

2.1 Theory

The open circuit voltage, E_{cell}, for an electrochemical cell is related to the changes in Gibbs free energy (G), enthalpy (H), and entropy (S) of the associated reactions given by:

$$\Delta G = \Delta H - T\Delta S_{cell} = -nFE_{cell} \quad (1)$$

* shannon.yee@me.gatech.edu phone:1-404-385-2176 fax: 1-404-894-8496 www.yeelab.gatech.edu

where T is the temperature of the cell, n is the stoichiometry of the electrons transferred between the half-cell reactions that comprise the electrochemical cell, ΔS_{cell} is the entropy change associated with the half-cell reactions, and F is the Faraday constant. This equation states that any electrochemical reaction involves some heat exchange between the cell and its surroundings. This exchange, which is depicted by $T\Delta S_{cell}$, may be heat absorption or heat rejection depending on the sign of ΔS_{cell}. Positive and negative ΔS_{cell} are associated with heat rejection (endothermic) and heat absorption (exothermic) processes, respectively. Therefore, a reversible electrochemical cell that releases heat as it discharges at a certain voltage will, at the same pressure and temperature, absorb the same amount of heat as it charges at the same voltage.[7] Using this reversible isothermal heat exchange process, a continuous flow electrochemical cooling cycle can be envisioned as illustrated in Figure 1.

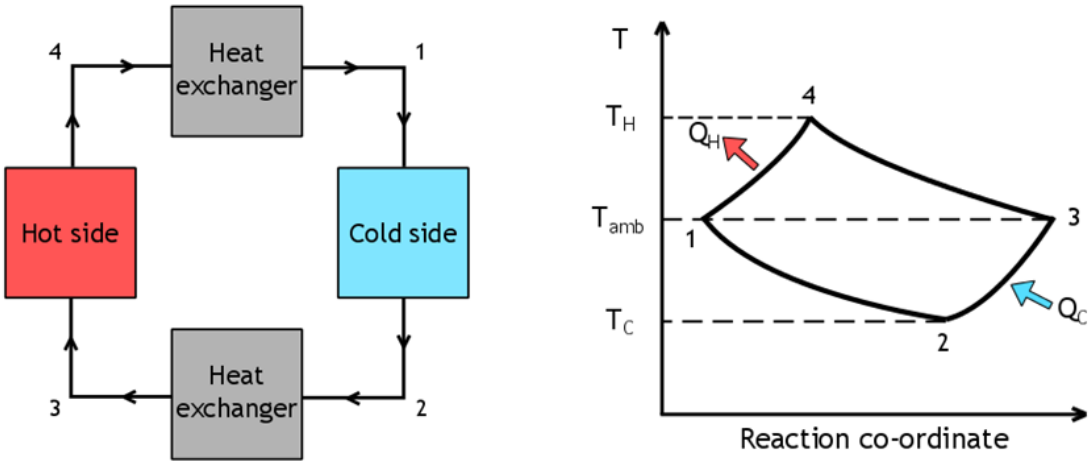

Figure 1. (a) Schematic showing the envisioned configuration capable of continuously cooling a source fluid. (b) The associated T-s diagram of the schematic in (a). The numbers in both panels map to each other. Q_C and Q_H represent the amount of heat absorbed from the source fluid and rejected into the sink fluid respectively.

As demonstrated in Figure 1a, this system entails two electrochemical cells that serve as the hot and cold sides, and two heat exchangers. In the cold side, appropriate half-cell reactions undergo endothermic electrochemical charging or discharging. The electrolytes, which function as the working fluid of the refrigeration system, leave the cold side at a temperature (T_C) lower than what they entered at. They then enter a heat exchanger where they cool the source fluid. The source fluid is inlet at ambient temperature (T_{amb}) and undergoes a temperature depression in the aforementioned heat exchanger. The electrolytes then enter the hot side where they undergo exothermic electrochemical charging or discharging. They leave the hot side at temperature T_H which is hotter than what they entered the hot side at T_{amb}. Subsequently, they enter the second heat exchanger where they reject their heat to a sink fluid and attain temperature T_{amb}. The sink fluid is also inlet at T_{amb} and leaves the heat exchanger at an elevated temperature. Depending on the sign of ΔS_{cell} for the half-cell reactions chosen, the hot side undergoes electrochemical charging or discharging to source an exothermic process. The cold side then undergoes the other process which sources an endothermic process.

The primary work input to the refrigeration cycle is dictated by the temperature coefficient of the half-cell reactions, α_{cell}. The change in open circuit voltage E_{cell} of the electrochemical cell is given by[7,8]

$$\alpha_{cell} = \alpha_{cathode} - \alpha_{anode} = \left(\frac{\partial E_{cell}}{\partial T}\right)_P = \frac{\Delta S_{cell}}{nF} \tag{2}$$

where $\alpha_{cathode}$ and α_{anode} are the temperature coefficients of the half-cell reactions occurring at the cathode and anode respectively. The voltage sourced by the discharging electrochemical cell can be redirected to the charging electrochemical cell such that the electrical work input is $\alpha_{cell}\Delta T$. $\alpha_{cell}\Delta T$ is the difference between the voltages, which is needed by the cold side E_c and is provided by the hot side E_h, such that $E_c - E_h = \alpha_{cell}\Delta T$.[8] This is in addition to the power required to pump the electrolytes in the system.

2.2 Designing a refrigeration cycle

We first chose half-cell reactions that would comprise the electrochemical cell. We looked at over 300 half-cell reactions, filtering those that would maximize the α_{cell} value. While α_{cell} dictates how much heat is absorbed per reaction, it provides no insight into the kinetic parameters which govern how fast heat is consumed or generated. Also, several half-cell reactions evolve gases and/or precipitates which could complicate the infrastructure of our device. Owing to its well-reported kinetics and relatively high α_{cell}[9,10], we opted to base our refrigeration system on the Vanadium Flow Redox Battery (VFRB).

The simplified half-cell reactions occurring in a VFRB are as follows[11]:

Cathode: $VO^{2+} + H_2O \underset{discharge}{\overset{charge}{\rightleftharpoons}} VO_2^+ + e^- + 2H^+$ E^Θ=1.004 V α = -0.9 mV/K

Anode: $V^{3+} + e^- \underset{discharge}{\overset{charge}{\rightleftharpoons}} V^{2+}$ E^Θ= - 0.255 V α = 1.5 mV/K

where E^Θ is the standard reduction electrode potential of the half-cell reaction. Both α and E^Θ are measured at pH = 0. Since α_{cell} is negative, electrochemical discharge occurs on the hot side, and the reactions marked charge occur on the cold side of the device. A design schematic of the device is shown in Figure 2 below. The green colored region indicates the electrolyte species undergoing the cathode half-cell reaction. The blue colored region indicates the electrolyte species undergoing the anode half-cell reaction. These are called the catholyte and anolyte, respectively. The orange region represents the proton exchange membrane (PEM). The top and bottom heat exchangers allow for heat exchange between the two electrolytes with the sink and source fluids, respectively. The electrolytes are prepared using hydrated vanadyl sulfate and 2M sulfuric acid. In the hot side, the V^{5+} present in the catholyte undergoes exothermic reduction to form V^{4+}. In the cold side, the applied potential forces the endothermic oxidation of the V^{4+} to V^{5+}. In contrast, the V^{2+} present in the anolyte undergoes exothermic oxidation to V^{3+} in the hot side. The V^{3+} undergoes endothermic reduction in the cold side to V^{2+}.

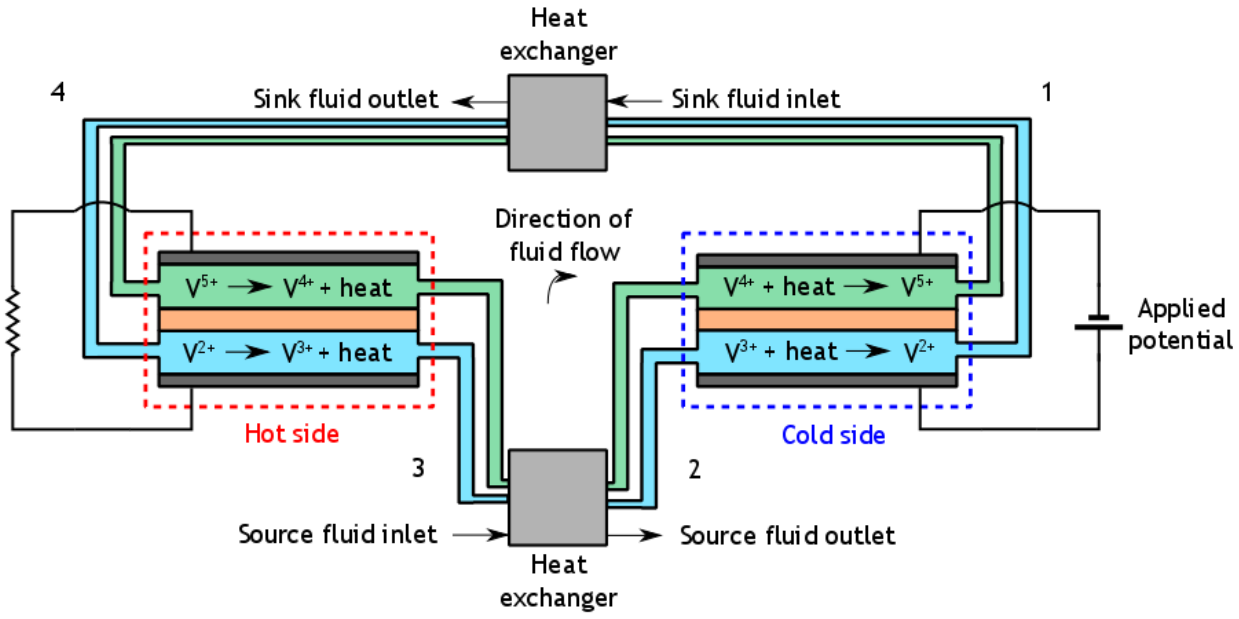

Figure 2. A detailed schematic of the vanadium flow electrochemical cooler. The catholyte and anolyte undergo reduction and oxidation respectively in the hot side; they undergo oxidation and reduction in the cold side respectively. More importantly, these processes are exothermic in the hot side, and endothermic in the cold side. The hot side is a thermodynamically spontaneous electrochemical cell. The open circuit voltage of the cell is less than the applied potential by a value of $\alpha_{cell}\Delta T$.

Similar to VFRBs, the above described vanadium flow electrochemical cooler is operated at constant current. It is obvious that the effectiveness of the device in cooling the source fluid is contingent on the depression in temperature of the electrolytes leaving the cold side. The current density is directly proportional to the rate of reactions at the hold and cold sides. However, it also results in greater Joule heating due to electronic and ionic currents. To find the optimal current density, we analyzed a steady-state finite difference model of the cold side. The schematic of the setup is shown in Figure 3 below. Table 1 shows the parameters used in the simulation.

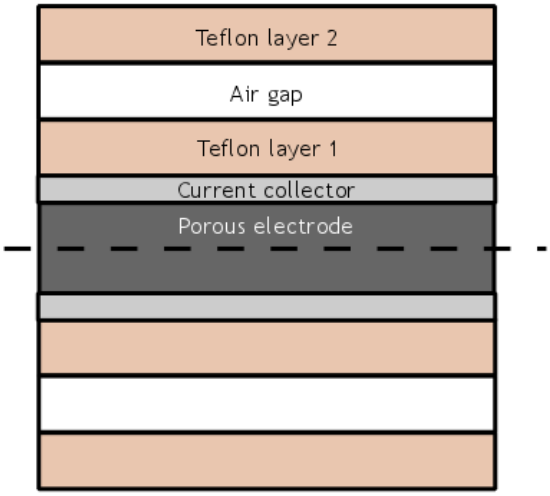

Figure 3. Schematic of the layers that house the cold side. The dotted line indicates the proton exchange membrane (PEM), which is an order of magnitude smaller than the electrode and is not included in the simulation. The layers are symmetric about the PEM. The stacks have 0.1 m long square cross-sections.

Table 1. Parameters used for the thermal finite difference model of the cold side[10]

Property	Symbol	Value	Property	Symbol	Value
Thickness		[mm]	Thermal conductivity		[W/m K]
Electrode	t_e	1.0	*Electrode*	k_e	0.15
Current collector	t_c	0.1	*Electrolyte*	k_l	0.67
Teflon layer 1	$t_{t,1}$	3.0	*Current collector*	k_c	16.00
Air gap	t_{air}	3.0	*Teflon*	k_t	0.25
Teflon layer 2	$t_{t,2}$	4.0	*Air*	k_{air}	0.02
Electronic and ionic resistance		[Ω m]	Heat transfer of ambient air	h	5 W/m^2 K
Electrode (electronic)	$\sigma_{e,e}$	0.002	Electrode thermal capacitance	C_e	4.19 MJ/m^3 K
Electrode (ionic)	$\sigma_{e,i}$	0.1	Porosity	ε	0.68
Current collector	$\sigma_{c,i}$	0.001	Electrode specific area	a_e	35000 m^{-1}

As per the schematic, the catholyte and the anolyte seep into the two porous electrodes on either side of the PEM on the left and exit on the right. The steady-state energy conservation equation may be written as follows,[12]

$$\nabla \cdot (C_e \boldsymbol{u} T) = \nabla \cdot (k \nabla T) + G \tag{3}$$

where $\boldsymbol{u}$, k and G represent the local electrolyte velocity, thermal conductivity, and heat generation terms. The latter is given by

$$G = \begin{cases} current\ collector: \sigma_c \left(\dfrac{I}{A_c} \right)^2 \\ cathode: (\sigma_{e,e} + \sigma_{e,i}) \left(\dfrac{I}{V_e a_e} \right)^2 - I\alpha_{cathode} T \\ anode: (\sigma_{e,e} + \sigma_{e,i}) \left(\dfrac{I}{V_e a_e} \right)^2 - I\alpha_{anode} T \end{cases} \quad (4)$$

where I, A_c and V_e represent the applied constant current, cross-sectional area of the stack and volume occupied by the porous electrode. The electrolytes entered the electrodes at 298 K and we calculate the average exit temperature of the electrolyte with varying current densities and flowrates. The current density was varied up to the limiting current density i_L corresponding to the flowrate. The limiting current density is the maximum achievable value for the parameter when the kinetics is governed by the bulk concentration of the limiting electroactive species, c_b. This value is given by[13]

$$i_L = nFk_m c_b \quad (5)$$

where k_m, the mass transfer coefficient, is given by[13]

$$k_m = 1.6 \times 10^{-4} u^{0.4} \quad (6)$$

The flow velocity, u, was assumed to be a uniform value in the electrode domains and zero everywhere else. The bulk concentration c_b was assumed to be 500 mol/m^3. We believe this is a reasonable, if not conservative, estimate going by the simulation results that used 1500 mol/m^3 as the initial concentration[10]. The results of the calculation are illustrated in Figure 4 below. The device is able to operate at high current densities because of the high specific area of the porous electrodes. The high specific area ensures that the limiting current density for a given flowrate is lower than the current density that results in more Joule heating than entropic heat absorption. It is obvious that lower flowrate allows for lower electrolyte exit temperatures, however, it also implies a lower limiting current density.

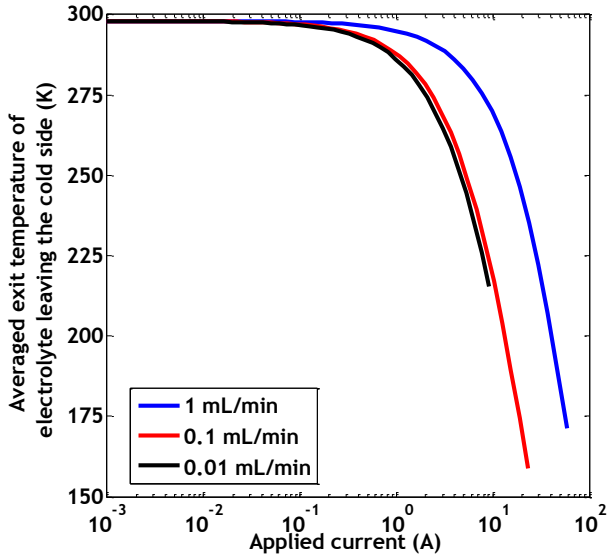

Figure 4. Variation of the average cold side exit temperature of the electrolytes with current density. The electrolytes enter the cold side at 298 K and undergo a depression in temperature due to the endothermic changes in entropy. For each flowrate, the current density is swept up to the corresponding limiting value at dictated by equation 3.

Keeping in mind the key ideas of discarding the heat absorbed by the electrolytes in the hot side and lowering the temperature of the electrolytes exiting the cold side, we arrived at a CAD design of the complete device as shown in Figure 5 below. The hot side is made out of a thermally conductive plastic that is resistant to sulfuric acid so as to discard some heat gathered by the electrolyte. The heat exchanger accounts for any remaining heat exchange to drop the temperature of the electrolyte leaving the hot side to ambient temperature. The cold side, however, is insulated to allow for the exiting electrolyte to be as cold as possible. The heat exchangers permit serpentine electrolyte and water streams to exchange heat through a thin tantalum coated copper sheet. We also use a Viton rubber gasket to ensure air tightness.

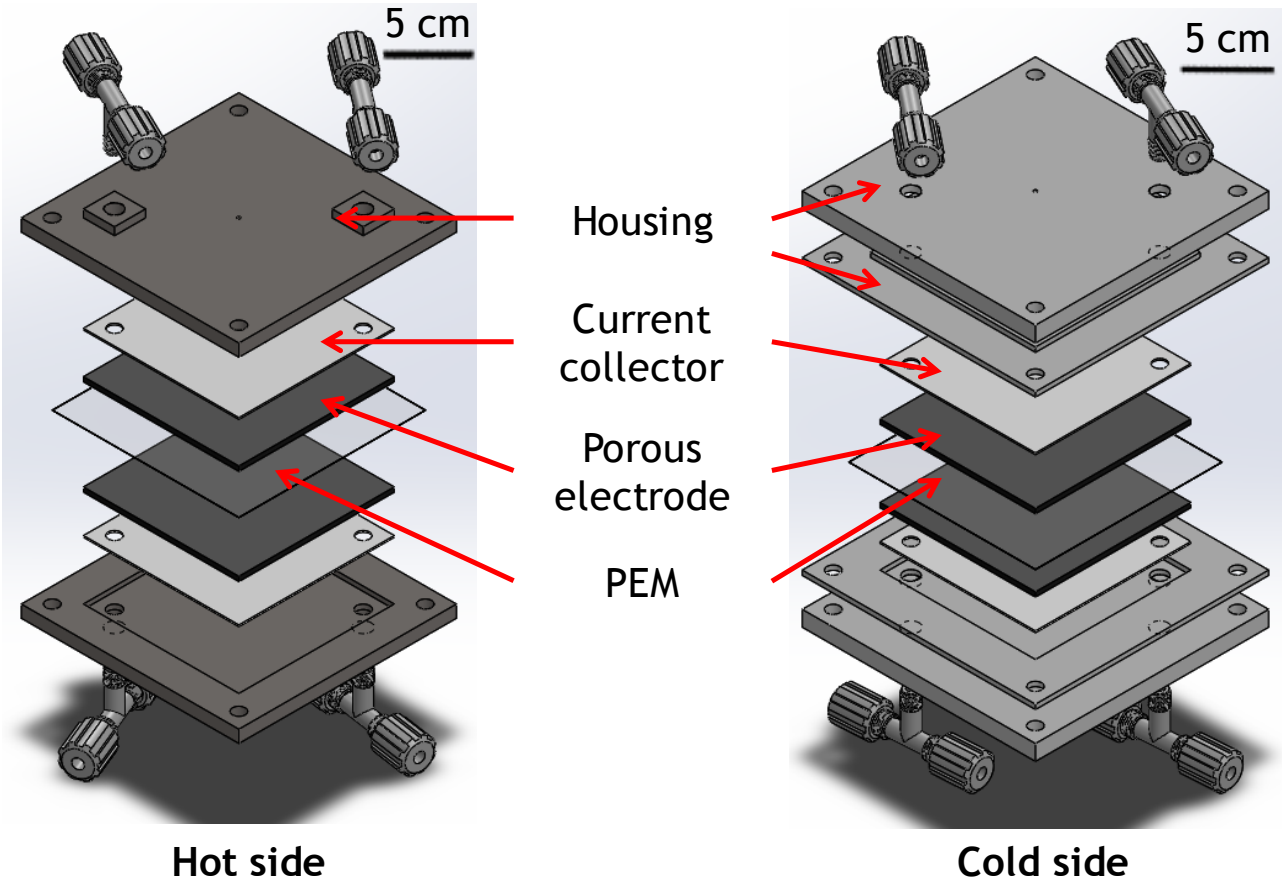

Figure 5. CAD design of the hold and cold sides of the electrochemical cooling device. Both devices are symmetric about their respective Nafion membranes. The cold side has additional housing components to reduce the amount of heat being absorbed from the environment.

3. SUMMARY

This paper has described preliminarily analysis and principal of an on-going cooling efforts outside the convention of typical bismuth telluride thermoelectric devices. As an alternative to solid-state thermoelectric devices, we have shown that thermo-electrochemical cell based on vanadium flow battery may have potential in cooling applications. The simple simulation that we performed suggest that there is an optimum ratio between the flowrate and the limiting current density of the cell, which will result in an optimum cooling performance. We hope that further research in this field will improve our understanding of the energy and heat transfer mechanisms underlying thermo-electrochemical cooling and provide alternative approaches for future researchers and engineers to further optimize this technology.

REFERENCES

[1] US Department of Energy, “Energy Savings Potential and RD&D Opportunities for Non-Vapor-Compression HVAC Technologies,” Report, March 2014, <https://energy.gov/eere/buildings/downloads/non-vapor-compression-hvac-technologies-report> (3 January 2017)

[2] Chein, R. and Huang, G., "Thermoelectric cooler application in electronic cooling," Appl. Therm. Eng. 24(14–15), 2207-2217 (2004).

[3] Riffat, S. B. and Ma, X., "Thermoelectrics: a review of present and potential applications, " Appl. Therm. Eng. 23(8), 913-935 (2003).

[4] Yang, J. and Stabler, F. R., "Automotive applications of thermoelectric materials," J. Electron. Mater. 38(7), 1245-1251 (2009).

[5] LeBlanc, S., Yee, S. K., Scullin, M. L., Dames, C. and Goodson, K. E., "Material and manufacturing cost considerations for thermoelectrics," Renew. Sust. Energ. Rev. 32, 313-327 (2014).

[6] US Department of Energy, “EERE Success Story—Xergy Develops Breakthrough Water Heater Compressor,” Slate, 15 September 2015, <https://energy.gov/eere/success-stories/articles/eere-success-story-xergy-develops-breakthrough-water-heater-compressor> (3 January 2017)

[7] Gerlach, D. W., [An Investigation of Electrochemical Processes for Refrigeration], University of Illinois at Urbana-Champaign, Urbana-Champaign (2004).

[8] Gerlach, D. W. and Newell, T. A., "Basic modelling of direct electrochemical cooling," Int. J. Energy Res. 31(5), 439-454 (2007).

[9] Shah, A. A., Watt-Smith, M. J. and Walsh, F. C., "A dynamic performance model for redox-flow batteries involving soluble species," Electrochim. Acta 53(27), 8087-8100 (2008).

[10] Oh, K., Yoo, H., Ko, J., Won, S. and Ju, H., "Three-dimensional, transient, nonisothermal model of all-vanadium redox flow batteries," Energy 81, 3-14 (2015).

[11] Bratsch, S. G., "Standard electrode potentials and temperature coefficients in water at 298.15 K," 18(1), 1-21 (1989).

[12] Moran, M. J. and Shapiro, H. N., [Fundamentals of Engineering Thermodynamics], 5th ed., John Wiley & Sons, Inc., West Sussex, UK, 2006

[13] Chen, J. Y., Hsieh, C. L., Hsu, N. Y., Chou, Y. S. and Chen, Y. S., "Determining the Limiting Current Density of Vanadium Redox Flow Batteries," Energies 7(9), 5863-5873 (2014).